Journal of Magnetic Resonance 300 (2019) 41–50

Contents lists available at ScienceDirect

Journal of Magnetic Resonance

journal homepage: www.elsevier.com/locate/jmr

Satellite nutation of half integer quadrupolar nuclei: Theory and practice

W.M.J. Franssen, E.S. Blaakmeer, A.P.M. Kentgens *

Radboud University, Institute for Molecules and Materials (IMM), Solid State NMR, Heyendaalseweg 135, 6525 AJ Nijmegen, the Netherlands

ARTICLE INFO

Article history:
Received 17 December 2018
Revised 20 January 2019
Accepted 21 January 2019
Available online 23 January 2019

ABSTRACT

For quadrupolar spin systems, interpretation of solid state NMR spectra can be hampered by the presence of resonances from both satellite and central transitions. This is particularly true for disordered systems, where many different quadrupolar sites exist, which can have strongly different quadrupolar coupling constants. If second order effects are too strong for obtaining meaningful MAS, MQMAS or STMAS spectra, an approach is needed to successfully separate central and satellite transitions.

In this work, we provide a rigorous treatment of 2D quadrupolar nutation NMR for the study of central and satellite transitions in quadrupolar systems. Using this SATURN experiment (SAtellite Transition nUtation of quadRupolar Nuclei) spectral intensity can be assigned to contributions from either central or satellite transitions. We show that the experiment can be applied to any half-integer spin (3/2, 5/2, 7/2 and 9/2), and that spectra can be obtained that closely match simulations. We furthermore show that distributions in quadrupolar parameters do not hamper the assignment of central and satellite transitions from a SATURN experiment.

1. Introduction

Solid state NMR is routinely used for the study of materials owing to its sensitivity to local atomic structure and dynamics. In order to distinguish different atomic sites in a material, local parameters such as the shielding of the magnetic field (chemical and knight shift) and the electric field gradient (quadrupolar coupling, for $I > 1/2$ nuclei) are probed via their effect on the NMR spectra. In order to record NMR spectra from which specific parameters can be extracted, a suitable toolbox of experiments is needed. In the case of quadrupolar nuclei (which have a spin quantum number higher than 1/2), the quadrupolar coupling to the electric field gradient tensor is the most information-rich and sensitive probe of the local structure. However, complications in NMR experiments of these nuclei can occur due to existence of multiple allowed transitions. In well defined materials, the occurrence of these so-called satellite transitions are clearly distinguished from the more-easily probed central transitions, and present no problems for contemporary NMR methods.

However, additional complications arise when the material of interest is disordered. As atomic sites have a less uniquely defined character, it becomes hard to distinguish between the central transitions and satellite transition of the different sites of the material, especially when the strength of the quadrupolar interaction varies strongly between these sites. This is especially true for materials whose spectra consists of broad second order lineshapes, where MAS, MQMAS and STMAS experiments fail to resolve the lineshape due to the physical limits on the spinning speed [1–6]. In this case, a method is needed that can distinguish between central and satellite transitions, allowing proper assignment of any observed spectral intensities.

In a previous work, we introduced 2D nutation as a method to distinguish satellite and central transitions in the analysis of ^{35}Cl ($I = 3/2$) of a Ziegler-Natta catalyst adduct [7]. As the nutation experiment relies on RF field strength to probe NMR interactions, a wide range of quadrupolar coupling constants can be studied [8–14]. In the current work, we give a thorough background of the theoretical aspects of the experiment, and show that it can be used to analyse half-integer quadrupolar nuclei systems with any spin quantum number. This experiment, nicknamed SATURN (SAtellite Transition nUtation of quadRupolar Nuclei), is furthermore shown to be insensitive to distributions in quadrupolar parameters, which can occur for disorder sites.

2. Background

2.1. Theory

A 2D nutation pulse sequence consists of an excitation pulse that is incremented in length (t_1 dimension) followed by regular recording of the FID after this pulse (t_2) (see Fig. 1). For spin $I = 1/2$ nuclei, this pulse sequence is generally used to determine the RF field strength (B_1). This is because, if other interaction can

* Corresponding author.
E-mail address: a.kentgens@nmr.ru.nl (A.P.M. Kentgens).

https://doi.org/10.1016/j.jmr.2019.01.010
1090-7807/

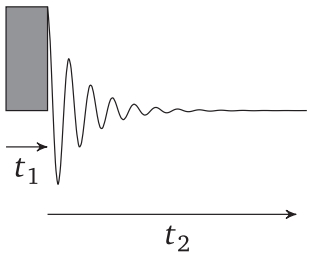

Fig. 1. Pulse sequence of a nutation experiment.

be ignored during the pulse (e.g. chemical shift, quadrupolar), the evolution of the observable magnetization M_{xy} during the pulse is equal to $M_{xy} = M_0 \sin(\omega_1 t_1)$, with M_0 the z-magnetization before the pulse, and ω_1 the B_1 field in rad/s. If such a nutation experiment is performed in the 2D fashion shown in Fig. 1, the spectrum will show only intensity at $F_1 = \omega_1/2\pi$, making extraction of the used RF field (and its homogeneity) straightforward. In this case, the appearance of the spectrum along F_1 does not hold information on the spin system, only on the used RF settings and B_1 inhomogeneity of the employed probehead.

In other cases, a significant broadening might be present (e.g. CSA, dipolar). In this case, a 2D nutation spectrum is affected by this interaction, as now the nutation is performed off-resonance, and the magnetization vectors rotate with a frequency determined by the effective field: $\omega_{\text{eff}} = \sqrt{\omega_1^2 + \omega_{\text{off}}^2}$. While the modulation along t_1 is affected by this offset, the experiment does not provide any new information on the system compared to a regular single pulse experiment.

In cases were a significant quadrupolar coupling is present, the effect of pulses becomes more involved. This fact is well known, and is often referred to as the 'solid' pulse length, taking into account that for a strong quadrupolar interaction relative to the RF field strength, the effective nutation frequency will be $\omega_1 \cdot (I + 1/2)$. If the nutation frequency of such a system is established to be a factor $(I + 1/2)$ higher than for a liquid state sample (using the same RF settings), it follows that the quadrupolar coupling constant of this site must be at least an order of magnitude larger than the used RF field strength. However, a more specific qualification of the quadrupolar coupling is not possible in this case.

In the intermediate case — were the RF and quadrupolar coupling strength are of the same order of magnitude — useful information can be extracted from the experiment. In this regime, both the central and satellite transitions intensities are modulated by multiple frequency components during the pulse. The amplitude and frequency of these modulations depend on both the RF field strength and the quadrupole interaction parameters. Using a known RF field strength, the size of the quadrupolar coupling can therefore be determined by observing the effect of pulses on the central transition, even if this transition does not display clear quadrupolar features in the regular NMR spectrum. In the following, we will show a more detailed analysis of the evolution of a half-integer quadrupolar spin system during a pulse, for this intermediate case.

If the quadrupolar coupling frequency is comparable to the applied RF field strength, the Hamiltonian during the pulse can be described as (for a spin 3/2 nucleus):

$$\begin{aligned}\mathcal{H} &= \mathcal{H}_1 + \mathcal{H}_Q^1 \\ &= -\omega_1 \cdot I_x + \Omega_Q(\theta,\phi) \cdot (I_z^2 - 5/4)/2 \\ &= -\omega_1 \begin{bmatrix} 0 & \frac{\sqrt{3}}{2} & 0 & 0 \\ \frac{\sqrt{3}}{2} & 0 & 1 & 0 \\ 0 & 1 & 0 & \frac{\sqrt{3}}{2} \\ 0 & 0 & \frac{\sqrt{3}}{2} & 0 \end{bmatrix} + \Omega_Q(\theta,\phi) \begin{bmatrix} \frac{1}{2} & 0 & 0 & 0 \\ 0 & -\frac{1}{2} & 0 & 0 \\ 0 & 0 & -\frac{1}{2} & 0 \\ 0 & 0 & 0 & \frac{1}{2} \end{bmatrix}\end{aligned} \tag{1}$$

with ω_1 the rf power in frequency units, and $\Omega_Q(\theta,\phi) = \frac{\omega_Q}{2}[(3\cos^2\theta - 1) + \eta_Q \cos 2\phi \sin^2\theta]$ with $\omega_Q = 3 \cdot C_Q/[2I(2I-1)]$ the angular independent quadrupolar frequency, and θ the polar and ϕ the azimuthal angle describing the orientation of the quadrupolar tensor in the magnetic field.

For the present discussion it is more convenient to work with a simplified view of the Hamiltonian, as for the moment we are only interested in the nature (zero or non-zero) of the elements, and not their exact value. The Hamiltonian of Eq. (1) in this representation becomes:

$$\mathcal{H} = \omega_1 \left[\begin{array}{cccc} \blacksquare & \square & \blacksquare & \square \\ \square & \blacksquare & \square & \blacksquare \\ \blacksquare & \square & \blacksquare & \square \\ \square & \blacksquare & \square & \blacksquare \end{array}\right] + \Omega_Q(\theta,\phi) \left[\begin{array}{cccc} \blacksquare & \square & \square & \square \\ \square & \blacksquare & \square & \square \\ \square & \square & \blacksquare & \square \\ \square & \square & \square & \blacksquare \end{array}\right] \tag{2}$$

were the black parts represent non-zero values, and the grey parts represent zeros.

During the pulse, the system evolves using this Hamiltonian. As the RF and quadrupolar part do not commute, the Hamiltonian must be transformed to a diagonal frame for viewing its effect. In this way, the Hamiltonian is expressed in a frame were the eigenfunctions of the Hamiltonian are used as a basis. We label this frame the 'nutation' frame. The Hamiltonian in this frame becomes:

$$\mathcal{H}^{(\text{nut})} = \left[\begin{array}{cccc} \blacksquare & \square & \square & \square \\ \square & \blacksquare & \square & \square \\ \square & \square & \blacksquare & \square \\ \square & \square & \square & \blacksquare \end{array}\right]. \tag{3}$$

This Hamiltonian propagates the density operator ρ, which, in thermal equilibrium ($t_1 = 0$) starts as:

$$\rho(0) = I_z = \left[\begin{array}{cccc} \blacksquare & \square & \square & \square \\ \square & \blacksquare & \square & \square \\ \square & \square & \blacksquare & \square \\ \square & \square & \square & \blacksquare \end{array}\right], \tag{4}$$

expressed in the rotating frame. To make the diagonal Hamiltonian work on this, it must be transformed to the same nutation frame (i.e. using the same basis):

$$\rho(0)^{(\text{nut})} = \left[\begin{array}{cccc} \square & \blacksquare & \square & \blacksquare \\ \blacksquare & \square & \blacksquare & \square \\ \square & \blacksquare & \square & \blacksquare \\ \blacksquare & \square & \blacksquare & \square \end{array}\right]. \tag{5}$$

In this frame, all the odd quantum coherences are populated, while the zero and double quantum terms are zero when starting from I_z. Each transition has been given its own colour, to distinguish them later on (this colour code is retained throughout this paper).

After the time t_1 in which the pulse is active, the experiment continues with a regular detection of the single quantum coherences (satellite and central transitions) in the rotating frame. For this, the evolved density operator $\rho(t_1)^{(\text{nut})}$ must be transformed back to the regular rotating frame.

For clarity, we will do this one element at a time. Taking the $2 \rightarrow 3$ transition:

$$\rho(t_1)_{2,3}^{(\text{nut})} = \left[\begin{array}{cccc} \square & \square & \square & \square \\ \square & \square & \omega t_1 & \square \\ \square & \omega t_1 & \square & \square \\ \square & \square & \square & \square \end{array}\right], \tag{6}$$

which evolves to a phase of $\omega_{2,3}t_1$. Transforming this back to the rotating frame gives (showing only the > 0 coherences):

$$\rho(t_1)_{2,3} = \quad (7)$$

where the lighter colours represent higher intensities, and darker colours lower intensities (the displayed example is for a case with an RF of 100 kHz and a quadrupole coupling of 200 kHz). From this, it follows that modulation of the $2 \rightarrow 3$ transition in the nutation frame leads to a modulation with $\omega_{2,3}$ of *all* the coherences in the rotating frame. This is a consequence of the mixing of all the Zeeman states to form the basis of the nutation frame. This means that a single pulse can excite coherences of any order, an effect that is used to excite multiple quantum coherences in an MQMAS experiment. This also means that the intensity of the central and the satellite transitions are modulated by the same frequency $\omega_{2,3}$ during t_1. Fourier transformation of the data along t_1 therefore gives a spectrum where all signals detected during t_2 have a peak at $\omega_{2,3}/2\pi$ along F_1.

Performing the same analysis for the other terms gives a similar result (using the colour code of Eq. (5)):

$$\rho(t)_{1,2} = \quad (8)$$

$$\rho(t)_{3,4} = \quad (9)$$

$$\rho(t)_{1,4} = \quad (10)$$

This leads to the observation that, during the pulse, both the central and satellite transition intensities in the rotating frame are modulated by the same — in this case four — frequencies. Note that the intensities of this modulation *are* different for the central and satellite transitions.

The frequency of the modulation of each term in the nutation frame, ω_{ij}, is determined by the ratio of the RF field strength and the quadrupolar frequency. The $\Omega_Q : \omega_1$ ratio determines the relative size of the I_z^2 and I_x term, determining the Eigenfunctions of the Hamiltonian (i.e. the total spin operator). Eq. (1) can therefore be more conveniently expressed as:

$$\begin{aligned}\mathcal{H} &= -\omega_1 \cdot I_x + \Omega_Q \cdot (I_z^2 - 5/4)/2 \\ &= -\omega_1 (I_x + \Omega_Q/\omega_1 \cdot (I_z^2 - 5/4)/2)\end{aligned} \quad (11)$$

From this it is clear that the eigenfunctions of the Hamiltonian are dictated by Ω_Q/ω_1, and that the eigenvalues are determined by Ω_Q/ω_1 and scaled by ω_1 (in a similar way that, for the Zeeman term, I_z determines the eigenfunctions, and the Larmor frequency is used to scale the eigenvalues to the correct unit). The nutation frequency for a specific transition $i \rightarrow j$ can than be expressed as: $\omega_{i,j} = \omega_1 \cdot \Xi(\Omega_Q/\omega_1)_{i,j}$. The function Ξ holds the differences between the unitless eigenvalues of the Hamiltonian (which require diagonalization, and depends on Ω_Q/ω_1). ω_1 scales these values to a frequency unit. If Ξ is calculated for a specific spin quantum number, the nutation frequencies for a given Ω_Q and ω_1 can be easily obtained. An example of this function for a spin 3/2 nucleus is given in Fig. 2.

A similar analysis can be performed for the amplitudes of these modulations. The amplitude of a modulation of a specific nutation transition on a term in the rotating frame is determined by several factors. Firstly, the population of a nutation state is determined by the starting operator (often I_z) and the way it is transformed to the nutation frame. The transformation is determined by the eigenvectors of the Hamiltonian, and thus by Ω_Q/ω_1. This coherence is modulated during t_1 and, after that, must be transformed back to the rotating frame. This is again fully determined by the same eigenvectors (determined by Ω_Q/ω_1). This leads to the conclusion that the amplitude of a specific nutation modulation of a transition in the rotating frame is determined by the starting operator and Ω_Q/ω_1.

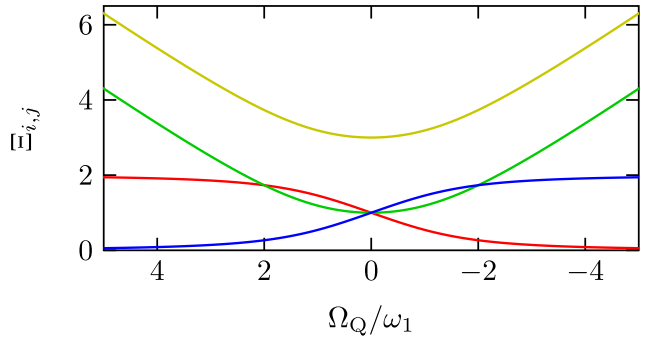

Fig. 2. Ξ-function for a spin 3/2 nucleus as function of the Ω_Q/ω_1-ratio. Coloured lines represent the different 1Q and 3Q nutation transitions with the same colour code as in Eq. (5). (For interpretation of the references to colour in this figure legend, the reader is referred to the web version of this article.)

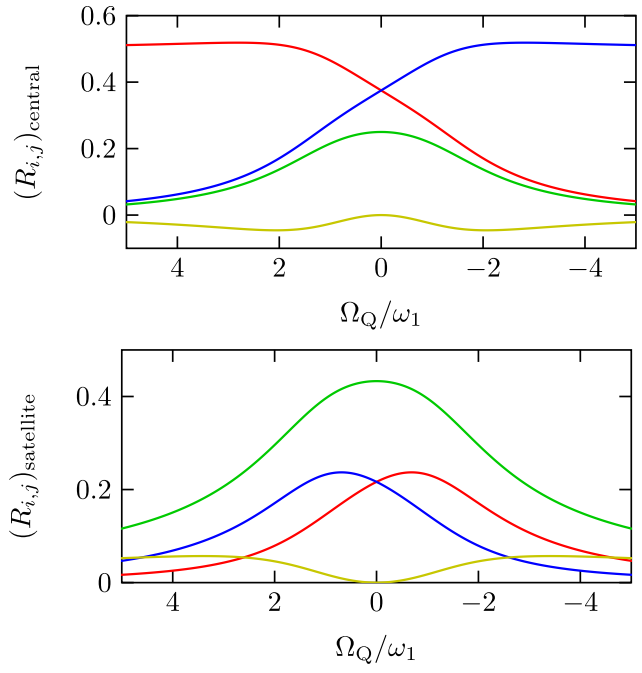

Fig. 3. *R*-values for each nutation transition (same colour code as in Eq. (5)) mapping to the rotating frame central (top) or satellite (bottom) transition for a spin 3/2 nucleus as function of the Ω_Q/ω_1-ratio starting from thermal equilibrium. (For interpretation of the references to colour in this figure legend, the reader is referred to the web version of this article.)

Together these effects are contained in the $(R_{i,j})_{k,l}$ factors [7,15]. These are the projection coefficients of a nutation coherence i,j to a coherence k,l in the rotating frame when starting from a specific initial state. Fig. 3 shows these R terms for all four nutation transitions of a spin 3/2 nucleus on the central and satellite transitions in the rotating frame ($(R_{i,j})_{2,3}$ and $(R_{i,j})_{1,2}$) when starting from thermal equilibrium (I_z). Note that the R factors are identical for the two satellite transitions 1,2 and 3,4.

From Figs. 2 and 3 a remarkable effect can be observed: while the central transition frequency of a quadrupolar nucleus is not affected by the first order quadrupolar coupling, the evolutions of the central transition intensity during a pulse is uniquely determined by the strength of this quadrupolar coupling, given a known RF field strength. In this way, the quadrupolar coupling can be extracted from the nutation spectrum of the central transition of a nucleus [9,10,16,11].

When performing a 2D nutation experiment on a spin 3/2 nucleus in a single crystal, this leads to the following effects. During t_1, the system evolves under the four nutation frequencies. During t_2 the system is modulated with three frequencies: $F_2 = 0$ for the central transition (assuming no second order effects, or chemical shift) and $F_2 = \pm\Omega_Q$ for the satellite transitions. A simulated example of the resulting 2D spectrum is shown in Fig. 4 (showing only the $F_1 < 0$ part). In this case, $\Omega_Q = 100$ kHz leading to a central transition at $F_2 = 0$ kHz, and satellite transitions at $F_2 = \pm 100$ kHz. Each of these transitions in F_2 shows three lines along F_1. The position of these lines are the same, as they result from projections of the same coherences during the pulse. However, the intensities will be different as they follow the R-factors depicted in Fig. 3. Note that, in this case, only the single quantum nutation transitions are observed as the triple quantum intensity is quite low.

In case of a powder, the resulting 2D nutation spectrum is naturally the sum of the spectra of the individual crystallites. Every crystallite has its own Ω_Q, depending on the C_Q and η value of the site, and the orientation of the tensor in the magnetic field (θ and ϕ). Along the direct dimension F_2, this means that all the central transitions are found near $F_2 = 0$, while the satellite transitions of each crystallite resonate at multiples of the quadrupolar coupling Ω_Q. This leads to the fact that the central transition intensity of all crystallites overlap in F_2, while forming a 'powder' pattern along the nutation dimension F_1 due to their distribution in Ω_Q (ω_1 is the same for all crystallites).

For the satellite transitions, a different effect occurs. The same nutation frequencies as for the central transition are observed, but they are now spread out over the satellite manifold along F_2.

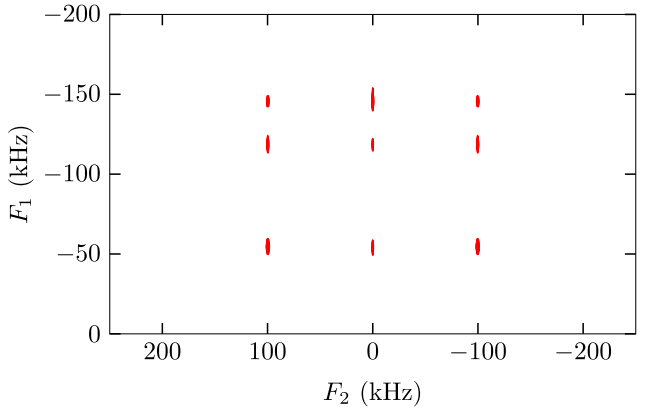

Fig. 4. 2D nutation spectrum of a $I = 3/2$ nucleus in a single crystal having $\Omega_Q = 100$ kHz using a RF field strength of 100 kHz. Only the $F_1 < 0$ part is shown.

Moreover, every position in the satellite manifold has a specific Ω_Q attached to it: only signals with $\Omega_Q = f$ have satellite intensity at $F_2 = f$. Therefore, moving along the satellite manifold in F_2 is equivalent to moving along the Ξ function: every point f along F_2 has its own Ω_Q/ω_1. This has the consequence that a 2D nutation spectrum of a powder shows the Ξ pattern of Fig. 2 for the satellites. This makes satellite transitions to be very recognizable in a 2D nutation spectrum, when compared to the central transition. An example of a simulated 2D nutation spectrum for a spin 3/2 nucleus is shown in Fig. 5a (ignore the other plots for now). Dividing both the x and y-axis by $\omega_1/2\pi$ will lead to the exact same shape as in Fig. 2. Note that, due to its low intensity, the 3Q nutation transition is not observed in Fig. 5a. The central transition shows a powder pattern along F_1, as was discussed above.

The fact that satellite transitions are very recognizable in a 2D nutation spectrum, allows for accurate assignment of any observed spectral intensity. This is particularly useful in cases with a distribution of quadrupolar parameters, were any overlap between a broad central transition (due to disorder combined with second order effects, CSA, dipolar interaction, etc.) and the satellites from another site can be hard to distinguish due to the ill-defined nature of the line shapes in a 1D experiment.

2.1.1. High order transitions

During t_2, only single quantum intensity can be observed, as is common for every NMR experiment (I_- as a detection operator). However, during the pulse the higher odd order quantum nutation transitions are populated (see Eq. (5)). As these transitions map to the rotating frame central and satellite transitions, higher order nutation resonances *are* observable, albeit with low intensity. This can be seen in Fig. 3, were the yellow nutation 3Q transition maps to the central and satellite transitions in the rotating frame with a reasonable amplitude. This means that, depending on the spin quantum number, there can be a large number of observable higher order nutation transitions.

Under normal conditions, when starting the experiment from thermal equilibrium, these higher order resonances are of low intensity, and only visible if a high SNR spectrum is recorded. However, if a non-equilibrium initial state is created, the intensity of these higher order nutation transitions can be strongly enhanced. A way to achieve such enhancements is by selectively inverting the central transition before the high power nutation pulse. In the Results section below, this is shown for a spin 5/2 nucleus.

2.1.2. Phase effects

During the application of a nutation pulse to a quadrupolar spin system, the satellite transitions appear to be off-resonance: they have a certain offset compared to the transmitter. This is a consequence of the effect of the quadrupolar coupling. The term 'off-resonance' is deceptive in this case: for a quadrupole system with a non-zero quadrupolar coupling, 'on-resonance' pulses are by definition impossible. The best we can do is to be on-resonance for a specific transition. As a result, the modulation during the pulse is not a pure amplitude modulation, but also has phase modulation character. The problem is that, while off-resonance manipulation of the satellites occurs, no fictitious spin 1/2 approximation can be used, as we are influencing all the transitions at the same time.

In order to separate these effects, it is convenient to first look at a 2D nutation experiment for a spin 1/2 system, with an inhomogeneously broadened line (e.g. due to chemical shift anisotropy). For the on-resonant part of the spin system, a regular nutation spectrum for a spin 1/2 nucleus is observed: a single peak at ω_1. For the off-resonant parts, the nutation frequency is equal to the effective field given by $\omega_{nut} = \sqrt{\omega_1^2 + \omega_{off}^2}$, with ω_{off} the offset frequency. This leads to a non-linear dependence of the nutation

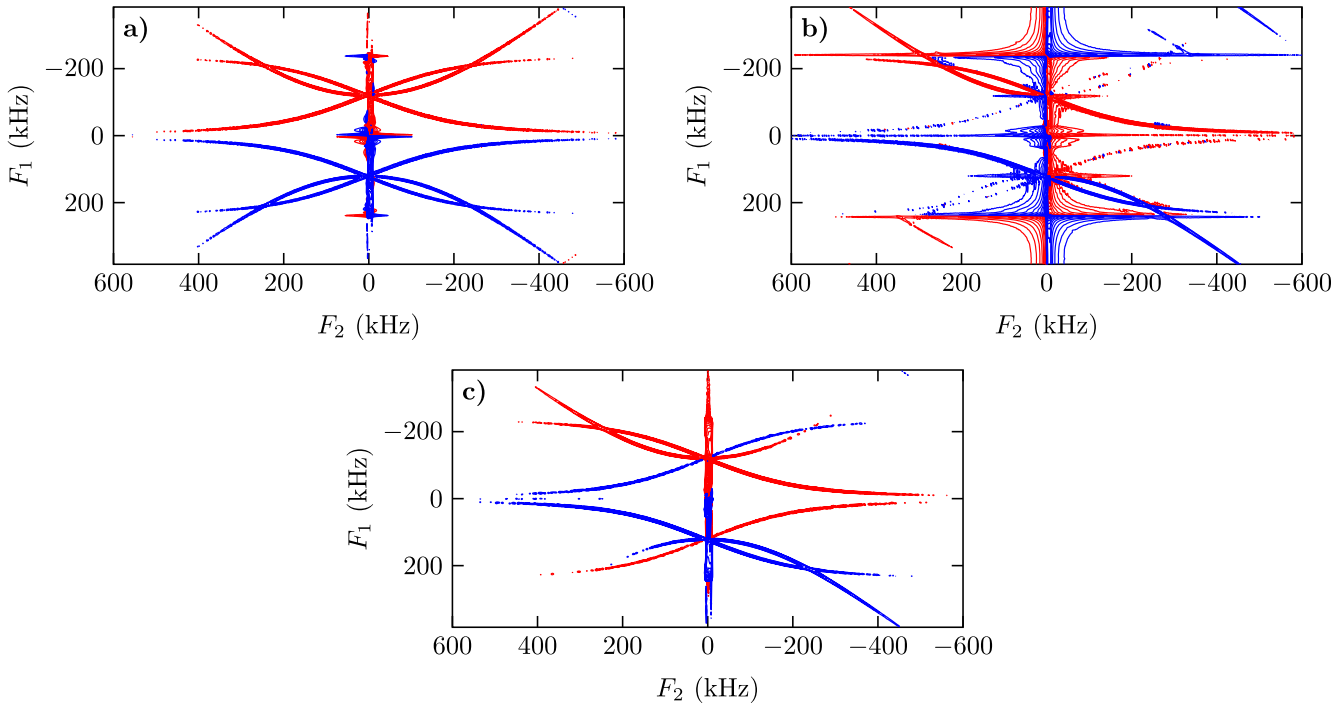

Fig. 5. Simulated ^{23}Na solid echo SATURN spectra of Na_2SO_4 ($C_Q = 2.6$ MHz, $\eta = 0.58$) at an RF field strength of 133 kHz RF at 9.4 T. (a): regular echo with real Fourier transform. (b): regular echo with complex Fourier transform. (c): whole echo with complex Fourier transform.

frequency as a function of the offset, which results in a characteristic 'smile' in the 2D nutation pattern of such a system.

Apart from a different size, the effective field also changes direction as a function of the offset. Depending on the RF field strength to resonance offset ratio, the effective field lies somewhere in the *xz*-plane. During the pulse, the magnetization precesses along a cone around this effective field. This means, after pulse time *t*, the magnetization does not always end op in the *yz*-plane, but can have any orientation. Depending on the size and direction of the effective field, the magnetization after the pulse will therefore have a certain phase in the *xy*-plane. Due to this, dispersive line shapes play a role along F_2 for each spectrum, distorting the phase of the 2D nutation spectrum. These dispersive line shapes are caused by the phase modulation of the detection signal (which is only amplitude modulated when on-resonance).

A second effect is that, due to this tilted effective field, some part of the initial magnetization is parallel to the effective field, and does not evolve during the pulse. This part, however, does have an *x*-component, leading to observable signal during F_2. In the 2D nutation spectrum, this signal is shown as a zero-frequency component along F_1. As essentially no information is contained is this part, an offset correction can be applied to the nutation time signal of every trace, removing this $F_1 = 0$ component.

These combined effects can be observed for the 2D nutation spectrum for the inhomogenously broadened spin 1/2 case shown in Fig. 6. Note that the CSA in this case is only used to create a series of spin 1/2 spins with a certain shift, to create the offsets. The shown off-resonant effects would be the same for a dipolar broadened system, or by measuring in an inhomogeneous magnetic field. As the offset changes direction when moving from $F_2 < 0$ to $F_2 > 0$, the spectrum shows inversion symmetry over the origin.

As described above, for a quadrupolar system, the 'off-resonance' effects are more difficult to judge due to the relation between the different transitions. However, when performing a quadrupole nutation experiment for satellite transitions, the resulting spectrum does show the effects as described for the spin 1/2 case: the phase of the signal in the F_2-domain depends on the effective 'offset' (i.e. the quadrupole coupling) and leads to dispersive signals. Moreover, there can be significant contributions of a zero frequency components along F_1. This latter effect can be corrected for by performing an offset correction for every time signal along t_1.

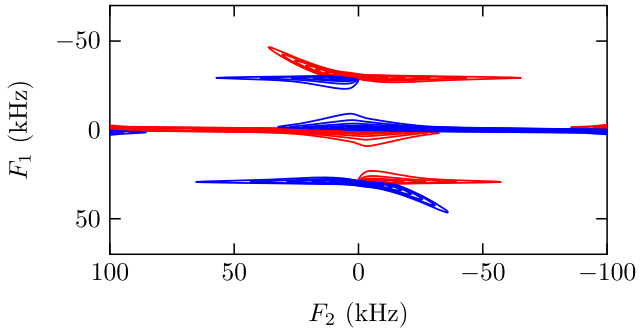

Fig. 6. SATURN spectrum of a CSA pattern ($\eta = 1$) using 30 kHz RF. Note the offset dependent nutation frequency, the dispersive components along F_2, and the substantial intensity around $F_1 = 0$.

2.1.3. Echo detection and real Fourier transform

In the previous Section, it is discussed that a 2D nutation experiment contains dispersive contributions along F_2 due to offset dependent phase distortions generated during the nutation pulse. In order to obtain a high resolution 2D nutation spectrum, these effects must be overcome. At this point, it is also important to realize that, in a realistic experiment, we are forced to use an echo sequence to record the signal. This is due to the dead time of the probe, which makes it impossible to record short-lived signals from broad satellite patterns.

If we indeed use an echo sequence to record the signal, it must be taken into account that the echo top will *not* form at $\tau_2 = \tau_1$. This is caused by the non-linear phase distortion created during the nutation pulse. Due to this, an imperfect refocussing takes place after $\tau_2 = \tau_1$. If the phase separation becomes too large (i.e.

for a long nutation pulse) no echo top will form for the satellites. This effect, however impeding it might sound, is actually a feature of the nutation experiment, and does not pose problems when correct processing is performed.

One way to remove the phase modulation behaviour is by performing a real Fourier transform along t_1 (i.e. set the imaginary part to zero prior to the transform). This leads to pure amplitude modulated data, and spectra with good resolution. Using this method, the spectrum has inversion symmetry over the line $F_1 = 0$ ($z(F_1, F_2) = -z(-F_1, F_2)$).

Another way to achieve suppression of the dispersive components is by using whole echo detection. In this experiment, the whole echo — rising and falling — is recorded. Swapping the echo around its top creates a symmetric signal around the acquisition centre, and leads to a spectrum where the dispersive components are removed [17]. Even though, in this case, the echo is quite asymmetric, a strong reduction of any dispersive components is still possible. This leads to a 2D nutation spectrum with better lineshapes, while retaining the information coded in the phase modulation along t_1. Spectra processed in this way show inversion symmetry with respect to the origin (i.e $z(F_1, F_2) = -z(-F_1, -F_2)$).

Fig. 5 shows simulated spectra for the different ways of acquiring and processing a 2D nutation spectrum for a spin 3/2 nucleus. When measuring a regular echo (i.e. not a whole echo), a Real Fourier transform is needed to obtain a high quality spectrum (compare Fig. 5a–b). This is due to the dispersive components discussed above. When recording the whole echo, a complex Fourier transform can be used (see Fig. 5c). Comparing (a) and (c), some key difference can be observed: while in (a) all the intensity is positive (for $F_1 < 0$), both positive and negative signals appear in (c). Also, while (a) is symmetric around $F_2 = 0$, (c) shows differences in absolute intensities for the different lines for $F_2 < 0$ and $F_2 > 0$. Due to these effects, we consider spectrum (c) to be more distinctive. For this reason we prefer the whole echo recording and complex Fourier transform method. Subsequent spectra in this paper will be processed in this way, and we will only show the $F_1 < 0$ part from now on.

2.2. Processing

Processing of nutation spectra in general (i.e. for the central transition) is explained in Ref. [15]. Here the steps for processing the 2D nutation spectrum are summarized.

Firstly, the signal must be split at the echo top (in the whole-echo case). This can be done at the echo maximum of the first trace, although this is not the correct position as explained above. Further adjustments can be made using first order phase corrections. Fourier transformation gives the spectrum, which can be phased using zero order phasing. In the indirect dimension, all the traces should individually be corrected to decay to zero via an offset correction of the last part of the FID. After that, a row of zeros should be prepended to make the nutation interferograms start at $t_1 = 0$. Fourier transformation, and -90° zero order phasing then gives the 2D nutation spectrum. This processing can be repeated with different degrees of first order phasing in F_2, to recover the highest resolution in F_1. Naturally, the ideal echo centre should occur at $\tau_1 = \tau_2$, however, due to experimental delays this can be hard to find exactly. Do note that the proper first order phasing is always in such a way that the FID is shifted to the right (the echo maximum is reached later than $\tau_1 = \tau_2$).

2.3. Equipment

Recording satellite nutation spectra in principle requires no special equipment. However, for broad powder patterns, high RF fields might be necessary which requires a probe with a small diameter coil oriented perpendicular to B_0 [7]. Also, if high RF power pulses are used, pulse transients can be an issue, and might be avoided by frequency stepping at the end of the nutation pulse, as is shown in our previous work [8]. As RF-inhomogeneity is detrimental for a nutation experiment, the sample should be well inside the coil, and the coil itself should have enough turns.

3. Experimental

The experiments were performed on Varian VNMRS 7, 9.4, 14.1 T and 20 T systems, using Varian 3.2 mm T3 probes and a large volume rotor (9.4 and 14.1 T), and a T3 4.0 mm probe (20 T). The samples were: lithium borohydride ($LiBH_4$), potassium permanganate ($KMnO_4$, Aldrich, 97%), bismuth vanadium oxide ($BiVO_4$) and lithium niobium oxide ($LiNbO_3$, Alpha Aesar, 99.9995%). The nutation experiments were recorded using a solid echo pulse sequence (ϕ_{nut} = [0,180], ϕ_{echo} = [0,180], ϕ_{rec} = [0,0]). The same RF power was used for both the nutation and the echo pulse (calibrated on a saturated solution of $KMnO_4$ in water, or on the ^{79}Br signal of KBr for ^{51}V and ^{93}Nb). The pulse lengths of the echo pulses were: 3 μs for ^{7}Li, 1.7 μs for ^{55}Mn, 0.75 μs for ^{51}V, and 1.0 μs for ^{93}Nb. Inversion of the central transition for ^{55}Mn was performed using a 110 μs pulse with ~2 kHz RF power directly prior to the nutation pulse. The pulse length was optimized to give maximum satellite echo intensity in the first trace of the nutation experiment.

3.1. Simulations

The spectral simulations were performed using the SIMPSON software [18,19] (input scripts can be found in the SI) with as many as 196417 crystal orientations using the ZCW scheme [20]. As input parameters, the literature values for the quadrupolar parameters were used for Na_2SO_4 ($C_Q = 2.6$ MHz, $\eta = 0.58$ [21]), $BiVO_4$ ($C_Q = 5.08$ MHz, $\eta = 0.36$, −90 ppm CSA with $\eta = 0.4$ at (SIMPSON) angles $\alpha = 90^\circ, \beta = 60^\circ, \gamma = 76^\circ$ relative to the EFG tensor [22]) and $LiNbO_3$ ($C_Q = 22.1$ MHz, $\eta = 0.0$ [23]). For $KMnO_4$, values obtained in this work were used ($C_Q = 1.568$ MHz and $\eta = 0.121$). The experimental RF and echo values were used. For the inversion of the central transition, the starting operator was changed to account for an ideal inversion of the central transition. Simulations of the nutation frequency curves were performed using an in-house `Python` implementation of density matrix formalisms (available on request).

The Czjzek distribution spectra were simulated with SIMPSON using a pre-calculated distribution of C_Q and η, and using $d = 5$ [24]. The distribution had 10 steps in the η-direction and 50 in the C_Q. The highest C_Q value used was $5 \cdot \sigma$. For the simulation with $\sigma = 10$ MHz, the satellite transitions were not detected as this would lead to excessive folding. As the satellite signals are of very low intensity, no harm is done to the simulation in this case.

4. Results

4.1. Spin 3/2

Firstly, we will focus on the $I = 3/2$ case. As discussed above, in case of negligible second order effects, SATURN spectra should show the unique pattern found in Fig. 5. Fig. 7 shows the result of a ^{7}Li SATURN experiment for the hexagonal high-temperature phase of lithium borohydride ($LiBH_4$) at 110 °C. In this case, the quadrupolar coupling is small ($C_Q = 37$ kHz, $\eta = 0$ [25]), with a total width of about 20 kHz. Using a low RF field strength, the distinctive SATURN pattern can be clearly observed. In this case, recording the spectrum using MAS quickly leads to an averaging of the anisotropic effects, making it difficult to study the origin of

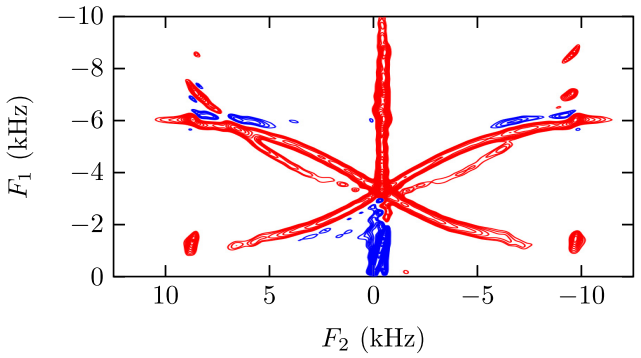

Fig. 7. ^{7}Li SATURN spectrum of $LiBH_4$ at 110 °C recorded using 3.3 kHz RF field strength at 7.4 T. In this case, regular echo detection and real Fourier transform have been used (compare to Fig. 5a).

any broader components (dipolar or satellites). Using a SATURN experiment with, in this case, ∼3 kHz RF field strength, the broader component can be readily assigned to satellite transitions.

4.2. Spin 5/2

The SATURN experiment can also be applied to nuclei with $I > 3/2$. We recorded spectra for the spin 5/2 ^{55}Mn nucleus in $KMnO_4$. For $I = 5/2$, there are five 1Q, three 3Q and one 5Q nutation transition. The central transition and both sets of satellite transitions will evolve with these same 9 frequencies during the nutation pulse (but with different amplitudes).

Naively, one might expect the SATURN spectrum to show a pattern of 9 lines, equivalent to the 4 transitions for spin 3/2 nuclei. However, for $I = 5/2$, there are two sets of satellites: one resonating at $\pm\Omega_Q$ and one at $\pm 2\Omega_Q$ along F_2. These lines have the same nutation frequencies, but different Ω_Q dependence in the direct dimension. This leads to two sets of 9 lines, of which those of the ±2 satellites have the same nutation frequencies as those of the ±1 satellites, but resonating at twice the frequency along F_2. A simulated and experimental SATURN spectrum of $KMnO_4$ is shown in Fig. 8. Also shown is a plot of all the 1Q nutation transitions for the ±1 and ±2 satellites. Note here that the ±2 satellites show the same pattern as the ±1, only scaled by a factor two along F_2. As the ±2 are more spread out, they are of lower intensity, and some of the lines are not visible at the signal-to-noise-ratio of the experimental spectrum. Apart from that, the experimental and simulate spectrum show nearly identical patterns.

4.3. Manipulation of the central transition

When manipulating a quadrupolar spin system, it should be realized that the individual transitions (central and satellites) can in general not be regarded as isolated. Only in the limit of low power RF pulses on a specific transition, the so-called fictitious spin 1/2 formalism holds [26]. But even then, swept pulses can be used to prepare a state with inverted satellite transitions leading to an enhanced population difference for the central transition (the double frequency sweep (DFS) sequence [27]). As nutation NMR with high power pulses mixes all the Zeeman states in the nutation space, preparing the systems before the nutation pulse is expected to have a more complicated effect.

As discussed above, the intensity of specific nutation transitions depend on the state of the system before the high power nutation pulse. Especially the higher order transition, which are of low intensity when starting from I_z, can be strongly enhanced by manipulating the central transition. One convenient way to achieve this is by inverting the central transition prior to the nutation pulse, which can be done by applying a soft, selective pulse on the central transition, in a similar way as has been described for the satellite transition by Wasylishen and coworkers [28].

Applying such an inversion pulse then leads to an alteration of the respective R-factors for, in this case, the spin 5/2 system. These

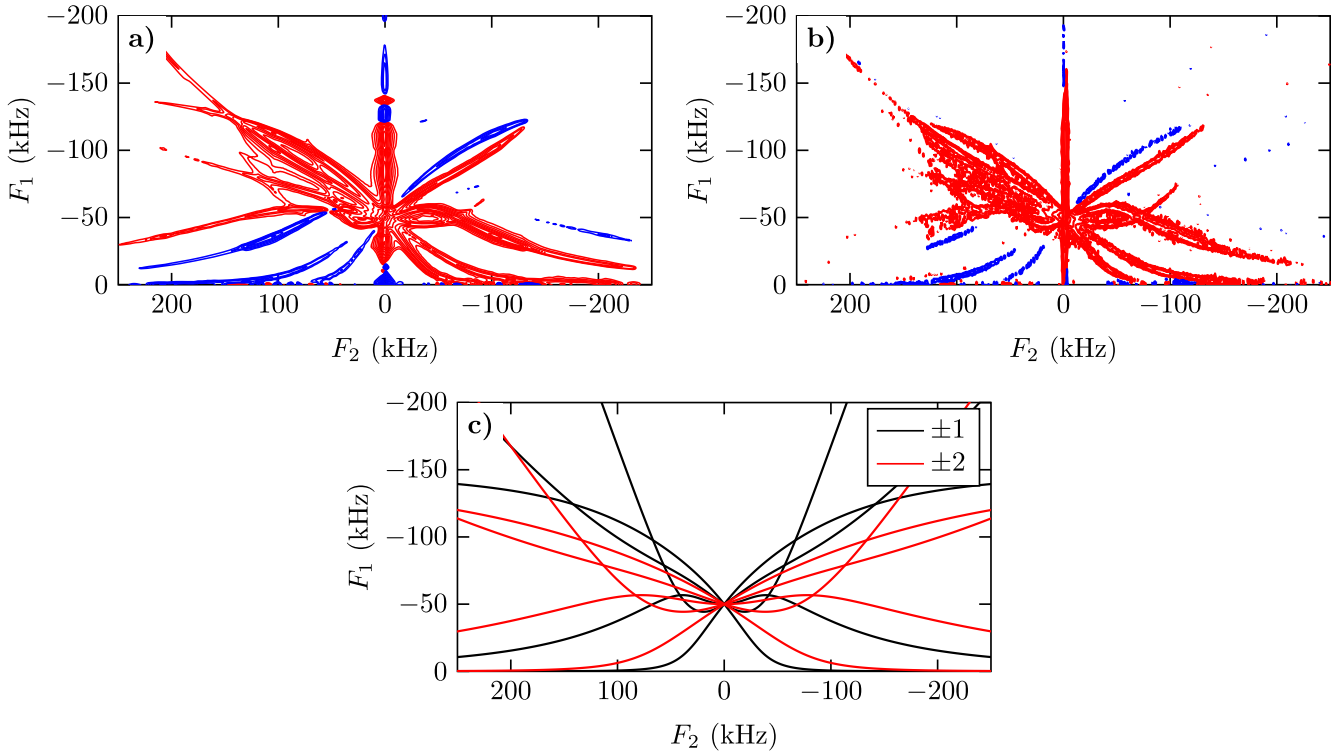

Fig. 8. Simulated (a) and experimental (b) ^{55}Mn whole echo SATURN spectra of $KMnO_4$ powder recorded with 50 kHz RF at 9.4 T. (c): Simulated positions of the single quantum nutation resonances, displaying the signals due to the ±1 and ±2 satellite transitions. Note that the pattern for the ±2 satellites is identical to those of the ±1 satellites, but stretched with a factor two along the x-axis.

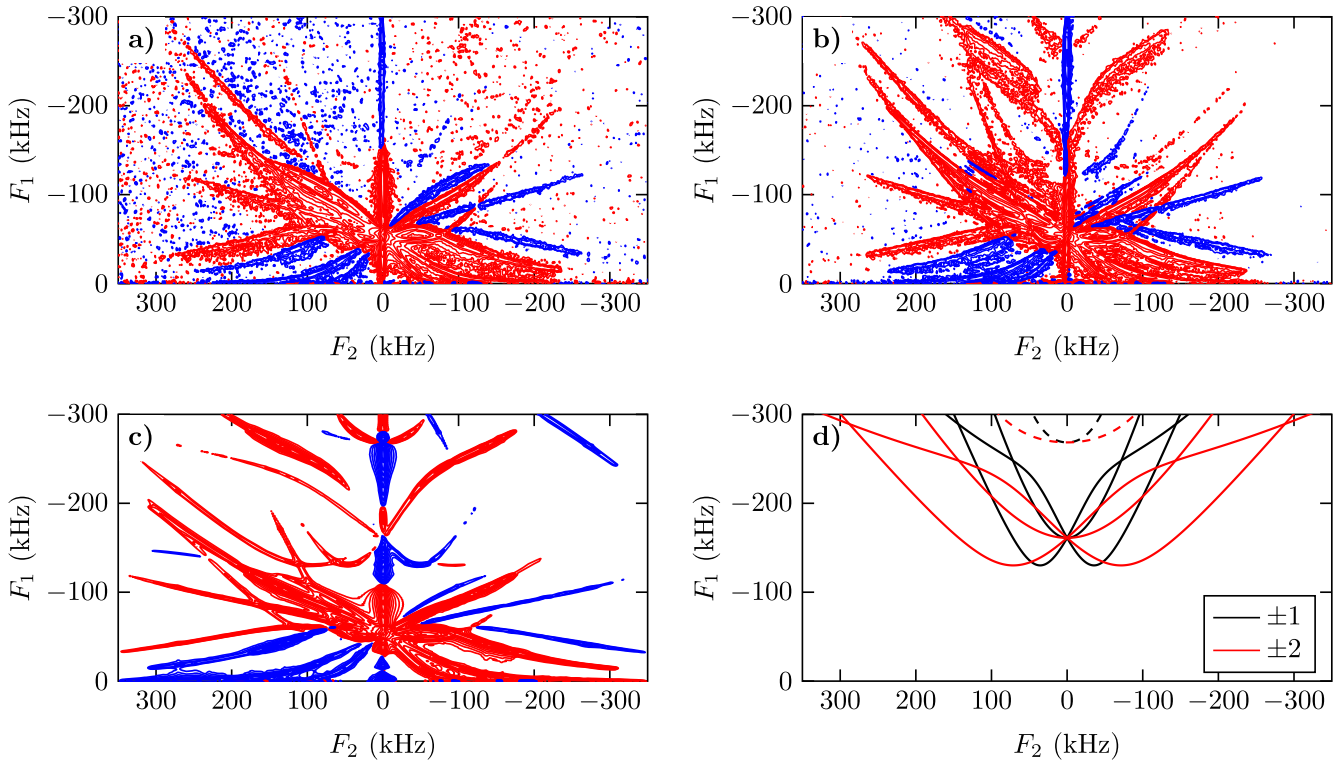

Fig. 9. ^{55}Mn whole echo SATURN spectra of $KMnO_4$ with 53.7 kHz RF at 14.1 T. (a): experimental without pre-inversion of the CT. (b): with pre-inversion. (c): simulation with ideal pre-inversion (negative lines coming from the top are due to aliassing). (d): 3Q (full) and 5Q (dashed) nutation transition energies for the ±1 and ±2 satellites. Also here, the pattern for the ±2 satellites is stretched with a factor two along the x-axis with respect to the pattern of the ±1 satellites.

factors are plotted in Fig. S1, and show about an order of magnitude enhancement for the 3Q and 5Q nutation transitions after inverting the central transition. Fig. 9 shows SATURN spectra for $KMnO_4$ without (a) and with (b) pre-inversion of the central transition. Moreover, a simulated spectrum for the inverted case is shown (c), as well as the theoretical nutation frequencies for the higher order nutation transitions (d). Comparing Fig. 9a and b, it is clear that the higher order transition are strongly enhanced in Fig. 9b. Note that even a 5Q nutation transition is now observable, as well as 3Q transitions from both of the sets of satellites.

4.4. Spin 7/2 and 9/2

Due to the fast increase of the number of nutation resonances and satellite transitions as a function of I, SATURN spectra of spin 7/2 and 9/2 systems will become quite complicated, with 21 and 36 single quantum nutation curves, respectively. However, as the highest order satellites are smeared out over a wide frequency range, the first and second satellites will be the most prominent, which leads to less complicated spectra than would be expected from this theoretical number of resonances.

Figs. 10 and 11 show experimental and simulated SATURN spectra for $I = 7/2$ (^{51}V in $BiVO_4$) and $I = 9/2$ (^{93}Nb in $LiNbO_3$). These show a good agreement between theory and experiment. For the spin 9/2 case, this particular sample has a faster relaxation decay during t_1, and does not have as high resolution along F_1 as the other examples. Nevertheless, the general shape is still identifiable, and the nutation pattern can be clearly distinguished from that of a central transition.

Similar to the spin 5/2 case, inversion of the central transition enhances the higher order nutation transitions. The R-factors can be found in Figs. S2 and S3 of the supplementary information, together with experimental spectra in Figs. S4 and S5.

4.5. Distributions in coupling parameters

In real-life systems, it is common to encounter situations were not one single well defined quadrupole interactions occurs for a

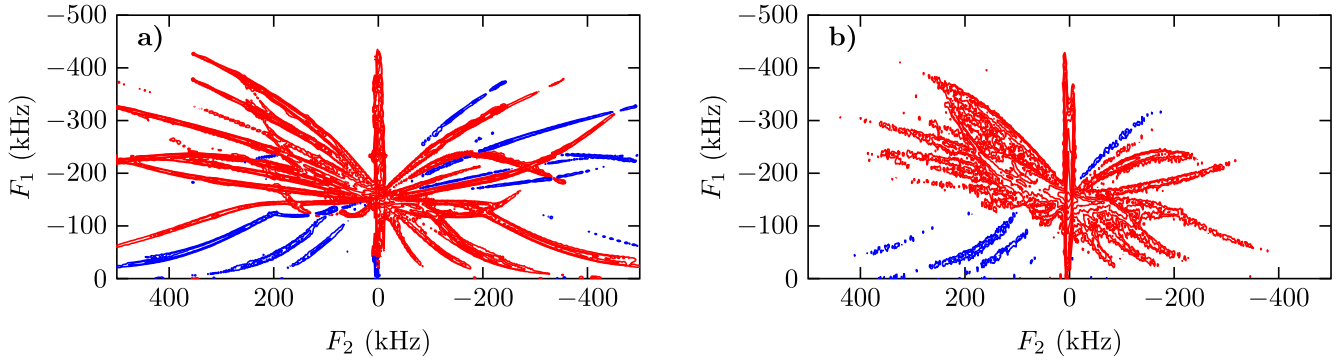

Fig. 10. Simulated (a) and experimental (b) ^{51}V SATURN spectra of $BiVO_4$ using 154 kHz RF power at 9.4 T.

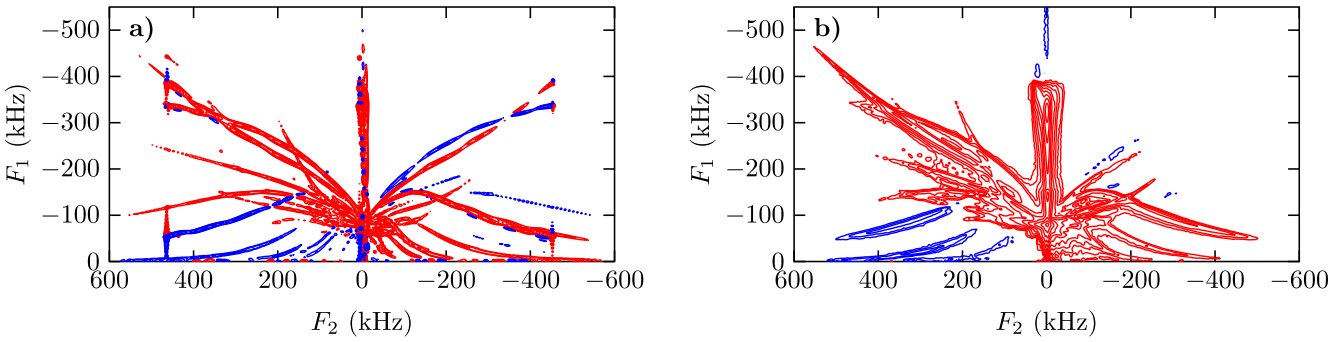

Fig. 11. Simulated (a) and experimental (b) ^{93}Nb SATURN spectra of $LiNbO_3$ using 78 kHz RF power at 20 T.

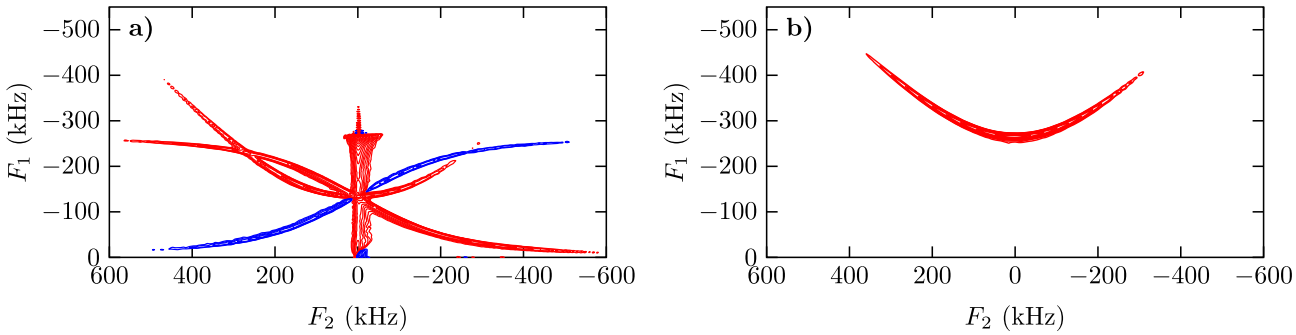

Fig. 12. Simulated SATURN spectra of a ^{23}Na Czjzek site with a small (left, 2 MHz) and high (right, 10 MHz) σ-value using 133 kHz RF power at 9.4 T.

given site. An example of such a case is an disordered system where the variation in quadrupolar interaction parameters can be described by a Czjzek distribution [29,30]. In these cases, multiple sites exist, with a distribution of quadupolar coupling parameters. Especially in these cases, assigning any observed featureless signal to a central or satellite transition can be difficult, as both a broad central transition and a satellite pattern can be the source of the observed signal.

This is were SATURN experiments are particularly useful as discussed in our study of the Ziegler-Natta catalyst [7]. Although there is a distribution in quadrupolar parameters, this does not pose a problem for our nutation experiment, as long as any second order and chemical shift effects are small when compared to the used RF field strength. Every signal at a position f in the satellite manifold experience the same Ω_Q, otherwise it would not resonate at that frequency. This means that all intensity from satellite transitions that resonate at this position is modulated in exactly the same way during the pulse (ω_1 and Ω_Q are the same for all signals that resonate at this position). This leads to the fact that a distribution in quadrupolar parameters does not change the appearance of the SATURN spectra, as long as ω_1 is larger than any second order quadrupolar effects.

Two extreme cases for a SATURN experiment for systems with a distribution in quadrupolar interactions parameters described by a Czjzek distribution are shown in Fig. 12. In Fig. 12a a simulation is shown for the case were the second order quadrupolar effects are small. In this case, a regular SATURN pattern is observed, despite of the presence of a distribution in C_Q. In Fig. 12b, the σ-parameter of the Czjzek distribution [30] is large, leading to a quadrupolar distribution with large C_Q values. This results in strong second order quadrupolar broadening of the central transition, and thus only an effective field effect is observed for the central transition ($\omega_{nut} = \sqrt{\omega_1^2 + \omega_{off}^2}$). In this case, the satellite transitions would be too smeared out to be visible in the spectrum.

In particular cases, the system that is analysed might have sites with very different quadrupolar interaction parameters, i.e. resonances from sites with small and large C_Q values are simultaneously present in the spectrum. The observed nutation spectrum for such a system might look like the sum of Fig. 12a and b. The contribution of the satellites of Fig. 12a are directly identified in the SATURN spectrum, making it possible to assign the observed spectral intensity to a sum of satellite and central transition contributions of two different sites.

In this way, spectra of disorder systems can be probed with a SATURN experiment, and the satellite/central transition character of each spectral region can be obtained. We used this in our previous work for the study of a disordered $MgCl_2$ adduct, which served as a model system for a Ziegler-Natta catalyst [7]. There, we showed that the underlying broad component in the ^{35}Cl NMR spectrum was due to satellite transitions of the bulk chlorine of the $MgCl_2$ support, as no features related to a central transition were found to be part of the wide line component.

5. Conclusions

We have given a rigorous treatment of the 2D quadrupolar nutation NMR experiment (SATURN) for the study of central and satellite transitions in quadrupolar systems. Due to the different influence of the quadrupolar coupling on the central and satellite transitions, the evolution of observable magnetization during a pulse can be used to distinguish both types of transitions. When displayed as 2D contour plots, very characteristic patterns emerge for the satellite transitions.

An in-depth theoretical framework for the SATURN experiment has been presented, and spectra that conform to theory have been obtained for nuclei with $I = 3/2$, $5/2$, $7/2$, and $9/2$. Moreover, we showed that distributions in quadrupolar parameters (i.e. Czjzek)

do not hamper the assignment of satellite/central character of the observed resonances.

Acknowledgements

The authors would like to thank Gerrit Janssen and Hans Janssen for technical support. Sander Lambregts is acknowledged for recording the SATURN spectrum of h-$LiBH_4$. The Netherlands Organization for Scientific Research (NWO) is thanked for their financial support of the program The Graduate School for Molecules and Materials (WF). Moreover, NWO supported the solid-state NMR facility for advanced materials research.

Appendix A. Supplementary material

Supplementary data associated with this article can be found, in the online version, at https://doi.org/10.1016/j.jmr.2019.01.010.

References

[1] W.P. Power, High-resolution solid-state ^{23}Na NMR of anhydrous sodium sulfite, Magn. Reson. Chem. 33 (3) (1995) 220–223.
[2] A. Medek, J.S. Harwood, L. Frydman, Multiple-quantum magic-angle spinning NMR: a new method for the study of quadrupolar nuclei in solids, J. Am. Chem. Soc. 117 (51) (1995) 12779–12787.
[3] D. Massiot, B. Touzo, D. Trumeau, J. Coutures, J. Virlet, P. Florian, P. Grandinetti, Two-dimensional magic-angle spinning isotropic reconstruction sequences for quadrupolar nuclei, Solid State Nucl. Magn. Reson. 6 (1) (1996) 73–83.
[4] Z. Gan, Isotropic NMR spectra of half-integer quadrupolar nuclei using satellite transitions and magic-angle spinning, J. Am. Chem. Soc. 122 (13) (2000) 3242–3243.
[5] Z. Gan, Satellite transition magic-angle spinning nuclear magnetic resonance spectroscopy of half-integer quadrupolar nuclei, J. Chem. Phys. 114 (24) (2001) 10845–10853.
[6] K.J. Pike, S.E. Ashbrook, S. Wimperis, Two-dimensional satellite-transition MAS NMR of quadrupolar nuclei: shifted echoes, high-spin nuclei and resolution, Chem. Phys. Lett. 345 (5-6) (2001) 400–408.
[7] E.S. Blaakmeer, W.M.J. Franssen, A.P.M. Kentgens, Quadrupolar nutation NMR to discriminate central and satellite transitions: Spectral assignments for a Ziegler-Natta catalyst, J. Magn. Reson. 281 (2017) 199–208.
[8] W.M.J. Franssen, Y.L.A. Rezus, A.P.M. Kentgens, High radio-frequency field strength nutation NMR of quadrupolar nuclei, J. Magn. Reson. 273 (2016) 33–39.
[9] A. Samoson, E. Lippmaa, Central transition NMR excitation spectra of half-integer quadrupole nuclei, Chem. Phys. Lett. 100 (3) (1983) 205–208.
[10] A. Samoson, E. Lippmaa, Excitation phenomena and line intensities in high-resolution NMR powder spectra of half-integer quadrupolar nuclei, Phys. Rev. B 28 (11) (1983) 6567–6570.
[11] A.P.M. Kentgens, J.J.M. Lemmens, F.M.M. Geurts, W.S. Veeman, Two-dimensional solid-state nutation NMR of half-integer quadrupolar nuclei, J. Magn. Reson. 71 (1) (1987) 62–74.
[12] F. Geurts, A. Kentgens, W. Veeman, ^{27}Al nutation NMR of zeolites, Chem. Phys. Lett. 120 (2) (1985) 206–210.
[13] P. Kempgens, Semi-analytical description of the $S = 9/2$ quadrupole nutation NMR experiment: multinuclear application to ^{113}In and ^{115}In in indium phosphide, Magn. Reson. Chem. 53 (4) (2015) 261–266.
[14] P. Kempgens, Investigation of the central line of ^{11}B in hexagonal boron nitride by a one-dimensional single pulse nutation NMR experiment, Solid State Nucl. Magn. Reson. 47 (2012) 35–38.
[15] A.P.M. Kentgens, Quadrupolar nutation spectroscopy, in: Encyclopedia of Magnetic Resonance, John Wiley & Sons Ltd., 2011.
[16] P. Man, Investigation of the central line of ^{55}Mn in $KMnO_4$ by a two-dimensional NMR method, J. Magn. Reson. 67 (1) (1986) 78–90.
[17] R.R. Ernst, G. Bodenhausen, A. Wokaun, Principles of Nuclear Magnetic Resonance in One and Two Dimensions, Clarendon Press, Oxford, 1987.
[18] M. Bak, J.T. Rasmussen, N.C. Nielsen, SIMPSON: a general simulation program for solid-state NMR spectroscopy, J. Magn. Reson. 147 (2) (2000) 296–330.
[19] Z. Tošner, R. Andersen, B. Stevensson, M. Edén, N.C. Nielsen, T. Vosegaard, Computer-intensive simulation of solid-state NMR experiments using SIMPSON, J. Magn. Reson. 246 (2014) 79–93.
[20] V.B. Cheng, Investigations of a nonrandom numerical method for multidimensional integration, J. Chem. Phys. 59 (8) (1973) 3992.
[21] H. Koller, G. Engelhardt, A.P.M. Kentgens, J. Sauer, ^{23}Na NMR spectroscopy of solids: interpretation of quadrupole interaction parameters and chemical shifts, J. Phys. Chem. 98 (6) (1994) 1544–1551.
[22] P.R. Bodart, Y. Dumazy, J.P. Amoureux, C. Fernandez, Orientation of electric field gradient and chemical shift tensors in $BiVO_4$ at room temperature by ^{51}V NMR, Magn. Reson. Chem. 37 (3) (1999) 223–226.
[23] S. Prasad, P. Zhao, J. Huang, J.J. Fitzgerald, J.S. Shore, Niobium-93 MQMAS NMR spectroscopic study of alkali and lead niobates, Solid State Nucl. Magn. Reson. 19 (1–2) (2001) 45–62.
[24] B. Bureau, G. Silly, J.Y. Buzaré, B. Boulard, C. Legein, Nuclear magnetic resonance quadrupolar parameters and short range order in disordered ionic fluorides, J. Phys.: Condens. Matter 12 (26) (2000) 5775–5788.
[25] L.M. Arnbjerg, D.B. Ravnsbæk, Y. Filinchuk, R.T. Vang, Y. Cerenius, F. Besenbacher, J.-E. Jørgensen, H.J. Jakobsen, T.R. Jensen, Structure and dynamics for $LiBH_4$-LiCl solid solutions, Chem. Mater. 21 (24) (2009) 5772–5782.
[26] S. Vega, Fictitious spin 1/2 operator formalism for multiple quantum NMR, J. Chem. Phys. 68 (12) (1978) 5518–5527.
[27] A.P.M. Kentgens, R. Verhagen, Advantages of double frequency sweeps in static, MAS and MQMAS NMR of spin I = 3/2 nuclei, Chem. Phys. Lett. 300 (3) (1999) 435–443.
[28] T.T. Nakashima, K.J. Harris, R.E. Wasylishen, Pulse FT NMR of non-equilibrium states of half-integer spin quadrupolar nuclei in single crystals, J. Magn. Reson. 202 (2) (2010) 162–172.
[29] G. Czjzek, J. Fink, F. Götz, H. Schmidt, J. Coey, J.-P. Rebouillat, A. Liénard, Atomic coordination and the distribution of electric field gradients in amorphous solids, Phys. Rev. B 23 (6) (1981) 2513–2530.
[30] G.L. Caër, B. Bureau, D. Massiot, An extension of the Czjzek model for the distributions of electric field gradients in disordered solids and an application to NMR spectra of ^{71}Ga in chalcogenide glasses, J. Phys. Condens. Matter 22 (6) (2010) 065402.